

# Superconducting Detector That Counts Microwave Photons Up to Two

Andrii M. Sokolov<sup>1,2,\*</sup> and Frank K. Wilhelm<sup>1</sup>

<sup>1</sup> Theoretical Physics, Saarland University, Saarbrücken 66123, Germany

<sup>2</sup> Institute of Physics of the National Academy of Sciences, pr. Nauky 46, Kyiv 03028, Ukraine



(Received 2 April 2020; revised 6 October 2020; accepted 4 December 2020; published 22 December 2020)

We propose a detector of microwave photons that can distinguish the vacuum state, one-photon state, and the states with two or more photons. Its operation is based on the two-photon transition in a biased Josephson junction and detection occurs when it switches from a superconducting to a normal state. We model the detector theoretically. The detector performs with more than 90% success probability in several microseconds. The working frequency can be set at the design stage in the range from about 1 to 20 GHz.

DOI: 10.1103/PhysRevApplied.14.064063

## I. INTRODUCTION

Quantum optics deals with indivisible units of electromagnetic radiation on an elementary level. It is not restricted to optical frequencies or interactions with single atoms. In fact, the platform of circuit quantum electrodynamics based on guided microwaves and superconducting circuits containing Josephson junctions has proven successful in implementing the functionality necessary for quantum optics [1–3] and to reach unparalleled coupling strengths of microwave photons to matter [4,5]. It is also a successful platform for quantum computing [6]. Unlike natural atoms, the matter component of circuit quantum electrodynamics can be specially tailored to perform a certain function [1]. For example, one can design a counter of microwave photons that is based on Josephson junctions [3,7–20].

There are several reasons to have such a detector. At the end of a quantum microwave experiment one usually amplifies a signal and then measures its amplitude with a homo- or a heterodyne. To achieve a decent signal-to-noise ratio, several amplification stages are required. Moreover, a cold stage with a quantum-limited amplifier [21] is used. This requires bulky circulators and additional drive tones (see, e.g., Ref. [22]). In the optical range one usually uses a photon detector, which reacts to a certain amount of energy. Photodetectors were also demonstrated in the microwave range. In Refs. [12–14] quantum nondemolition detectors were demonstrated. In Ref. [11] a destructive detector was demonstrated that uses only coherent quantum dynamics and hence allows rapid resetting. In Ref. [16], dissipation engineering was used to implement a destructive detector. However, these detectors rely on the readout of an ancillary qubit and their use in the readout

of another qubit does not reduce overhead. Moreover, the detectors include circulators and a several-stage amplification sequence, which rules out the possibility for a compact design with the current technology. The destructive detector demonstrated in Refs. [9,10] is quite compact as it only requires a resonator coupled to a Josephson junction. However, it is slow, requiring seconds for a photon to be detected. Josephson photomultipliers (JPMs) [3,7] are especially compact, fast, and simple destructive detectors. Use of the JPM in a microwave quantum optics experiment allows one to avoid complex and bulky amplification and promises integration with cold classical electronics [23]. This might be useful for faster control and data acquisition, as well as for building quantum information processing devices with more qubits.

Most designs for microwave photodetectors demonstrated so far only discriminate the vacuum state versus the states with a nonzero number of photons, i.e., they are called vacuum detectors [24]. However, for certain applications, a detector that resolves the input photon number is desirable. In the dispersive readout with a photodetector [7,25,26], photon-number resolution can improve fidelity in certain schemes [27]. Other uses include optimal discrimination of coherent states [28] and characterization [29] of microwave single-photon sources [30,31]. Detectors of microwave photons that possess limited capabilities for number resolution have been demonstrated [13,14] and envisioned [9,12]. However, they have a large footprint and other disadvantages discussed before, and they are only able to either distinguish a certain Fock state against all other states [12,14], react to photon number above a threshold [9], or determine parity of the photon number [13]. The detector demonstrated in Ref. [15] resolves up to three photons, but relies on readout of an auxiliary qubit, includes a pump, and requires prior knowledge of the photon shape for optimal operation. No compact

\* andriy145@gmail.com

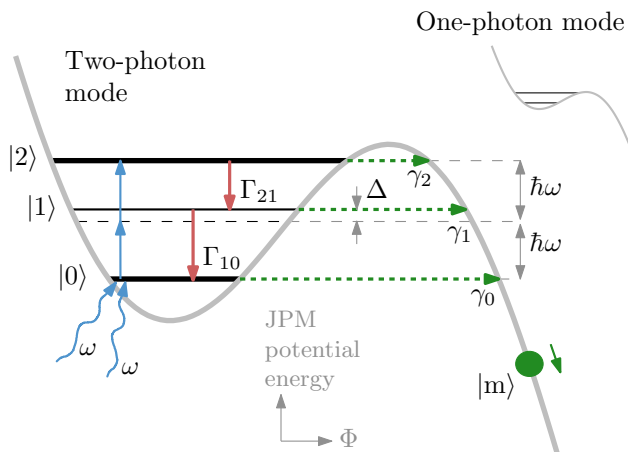


FIG. 1. Two modes of operation of the JPM that counts to two. In the two-photon mode, the JPM possesses three metastable states. A single photon rarely excites the JPM to  $|1\rangle$  due to detuning  $\Delta$ . Two photons excite it to  $|2\rangle$ , which then tunnels quickly to the (quasi)continuum. The JPM then “rolls” down the potential. This provides a macroscopic voltage on the junction, which is interpreted as a click. In the one-photon mode, the JPM possesses two metastable states. A single photon can deliver a click.

photodetectors with photon-number resolution have been demonstrated or proposed in the microwave range.

We propose a compact, photon-number-resolving JPM based on the two-photon transition (see Fig. 1). It works as follows. First the JPM is set in the two-photon mode and its ground state is prepared. In this mode, the JPM clicks if two or more photons are present. This can be seen as an extension of a vacuum detector. Note that, after a click, it is a slow process to return the JPM to a state where it is sensitive to photons. If there are fewer than two photons, the JPM is tuned to the single-photon mode. This can be done fast. Here it works as a vacuum detector and fires if a photon is present. Hence, the detector discriminates the vacuum state, single-photon state, and states with two or more photons. We provide a theoretical description of this detector in Secs. II–IV and evaluate its performance in Secs. V–VI.

## II. MODEL

In this section, we write out the Hamiltonian of our system. Then, we treat dissipation and tunneling with the Lindblad equation formalism. For simplicity, a current-biased Josephson junction (Fig. 2) serves as a JPM model. However, we discuss why our results are also applicable to the flux-biased JPM (Fig. 3).

### A. Hamiltonian

We consider a resonator coupled to a JPM (see Fig. 2). The full system Hamiltonian is

$$H = H_{\text{JPM}} + H_c + H_r. \quad (1)$$

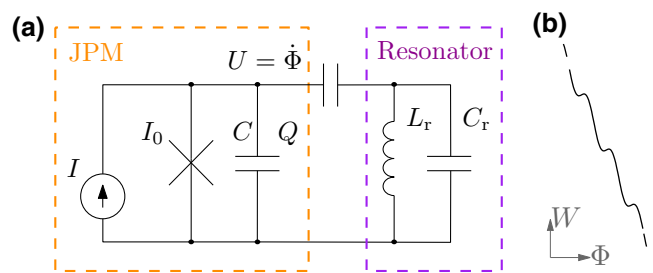


FIG. 2. (a) Circuit diagram of a resonator mode coupled to a JPM. The latter is a Josephson junction with a critical current  $I_0$  and contact capacitance  $C$ . The junction is biased with an external current  $I$ . Voltage  $U$  is read out by an external voltmeter. (b) The potential energy of the JPM.

Here, the resonator Hamiltonian is given by

$$H_r = \frac{Q_r^2}{2\tilde{C}_r} + \frac{\Phi_r^2}{2L_r}, \quad (2)$$

where  $Q_r$  denotes the charge on the resonator capacitance  $C_r$  and  $\Phi_r$  is the drop of quasiflux [32] on it. A tilde denotes that a capacitance is renormalized by the JPM-resonator interaction. The JPM Hamiltonian is of the form

$$H_{\text{JPM}} = \frac{Q^2}{2\tilde{C}} + W, \quad W = -\Phi_0 I_0 \cos \frac{\Phi}{\Phi_0} - I\Phi. \quad (3)$$

Here,  $\Phi_0$  denotes the flux quantum and  $Q$  is the charge of the JPM capacitance  $C$  with  $\Phi$  its quasiflux variable. The JPM resides in a washboard potential  $W$ , which is plotted in Fig. 1. The resonator and the JPM interact through a coupling capacitance  $C'$ . The coupling Hamiltonian is

$$H_c = \frac{\tilde{C}'}{CC_r} QQ_r. \quad (4)$$

The expressions for  $\tilde{C}$ ,  $\tilde{C}_r$ , and  $\tilde{C}'$ , as well as a detailed derivation of the circuit Hamiltonian are given in Appendix A. One can promote our canonical variables to

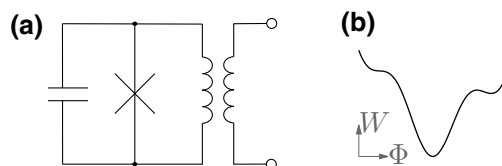


FIG. 3. (a) Another variant of JPM schematics: a flux-biased loop with a Josephson junction. (b) Energy landscape of this JPM variant.

operators. Their commutators are

$$[\Phi, Q] = [\Phi_r, Q_r] = i\hbar, \quad (5)$$

while the other pairs commute. For two related circuits, a similar Hamiltonian was obtained in Ref. [33], which only differs in the type of coupling.

It is convenient to rewrite the Hamiltonian (1) in terms of ladder operators. In the Hamiltonian model, we restrict the JPM dynamics to the metastable states in a well— $|0\rangle$ ,  $|1\rangle$ , and  $|2\rangle$  in Fig. 1. For the resonator, we make a usual substitution,  $\Phi_r = \sqrt{\hbar\rho/2} (a + a^\dagger)$  and  $Q_r = i\sqrt{\hbar/2\rho} (a - a^\dagger)$ , with  $\rho = \sqrt{L_r/\tilde{C}_r}$  the renormalized impedance of the resonator. The resulting Hamiltonian is

$$\begin{aligned} H = & \hbar(\omega + \Delta)|1\rangle\langle 1| + \hbar 2\omega|2\rangle\langle 2| + \hbar\omega a^\dagger a \\ & + \hbar g_1(|1\rangle\langle 0|a + \text{H.c.}) + \hbar g_2(|2\rangle\langle 1|a + \text{H.c.}), \end{aligned} \quad (6)$$

where  $g_1 = i\tilde{C}'(CC_r)^{-1}\sqrt{\hbar/2\rho}\langle 1|Q|0\rangle$  and  $g_2 = i\tilde{C}'(CC_r)^{-1}\sqrt{\hbar/2\rho}\langle 2|Q|1\rangle$ . The JPM is designed for its  $0 \rightarrow 2$  transition frequency to match  $2\omega$ , where  $\omega = 1/\sqrt{L_r\tilde{C}_r}$  is the resonator frequency. The rotating-wave approximation is used in obtaining the Hamiltonian. The coupling of the JPM to the resonator is assumed to be linear in the field quadrature; hence, its matrix elements in the Fock basis couple states that are different by exactly one photon.

## B. Lindbladian

The model given so far does not take into account the interaction with the external degrees of freedom. First, in Hamiltonian (6), we have excluded the states the system tunnels to. Hence, the tunneling is a nonunitary process in this model. Moreover, even the nontruncated Hamiltonian (1) does not take account of the nonradiative transitions in the JPM and its dephasing. However, it turns out that these processes, along with the tunneling, set the JPM performance.

To model them, we use the master equation formalism [34]. The Lindblad equation for our system reads

$$\dot{\rho} = L\rho, \quad L\rho = \frac{1}{i\hbar}[H, \rho] + (L_0 + L_1 + L_2)\rho. \quad (7)$$

Lindbladians  $L_0$ ,  $L_1$ , and  $L_2$  describe the incoherent processes involving the JPM states  $|0\rangle$ ,  $|1\rangle$ , and  $|2\rangle$ :

$$L_0 = \gamma_0 D[|m\rangle\langle 0|], \quad (8)$$

$$\begin{aligned} L_i = & \Gamma_{ii-1} D[|i-1\rangle\langle i|] + \Gamma_{ii} D[|i\rangle\langle i|] \\ & + \gamma_i D[|m\rangle\langle i|], \quad i = 1, 2. \end{aligned} \quad (9)$$

Losses in the resonator are neglected. Here  $D[\bullet]\rho = \bullet\rho\bullet^\dagger - \frac{1}{2}[\bullet^\dagger\bullet, \rho]_+$  with  $[a, b]_+ = ab + ba$ . For an  $i$ th excited state of the JPM,  $\gamma_i$  is its tunneling rate,  $\Gamma_{ii-1}$  is the relaxation rate, and  $\Gamma_{ii}$  is the pure decoherence rate. In abbreviations like these, we mean double index in a subscript. We denote by  $|m\rangle$  an amalgamation of the many possible states the JPM can tunnel into [8]. We have verified that a different tunneling model [35] does not change the main results of the paper.

## C. Flux-biased variation

A flux-biased loop with a junction [7] can be more convenient to operate. It avoids voltages above the gap and hence quasiparticle production; therefore, the JPM can be reset much faster. The circuit diagram of this JPM variant and its energy landscape is shown in Fig. 3. Here, tunneling occurs to bound states in the global minimum. One aims at a regime where the global minimum resides in a wide and deep well. Then it is unlikely for an excitation to bounce back to the local minimum and get re-emitted back to the resonator. In fact, there is a large number of densely separated bound states, which can be treated as a continuum. Tunneling here can be described in the same way as in the current-biased JPM we consider. Hence, we expect the same results for the flux-biased JPM variant.

## III. EFFECTIVE DESCRIPTION OF THE TWO-PHOTON PROCESSES

It is convenient to move to the frame where the first excited state of the JPM takes no part in the system dynamics. The two-photon terms appear then in the Hamiltonian explicitly. We use a Schrieffer-Wolff transform (see Ref. [36] and the references therein) to obtain the Hamiltonian in that frame. Also, one needs to know how the relaxation processes are dressed in this picture. Therefore, the very transform is also applied to the Lindbladian.

### A. Effective Hamiltonian

One can decouple the first excited state of the JPM with the unitary transform [37]

$$U = \exp(-\lambda_1|1\rangle\langle 0|a + \lambda_2|2\rangle\langle 1|a - \text{H.c.}), \quad (10)$$

where

$$\lambda_{1,2} = g_{1,2}/\Delta. \quad (11)$$

Hamiltonian (6) is then transformed as

$$\begin{aligned} H \rightarrow U^\dagger H U \approx & \hbar(\omega + \Delta + \chi_1)|1\rangle\langle 1| + \hbar(2\omega - \chi_2)|2\rangle\langle 2| \\ & + \hbar\tilde{g}(|2\rangle\langle 0|a^2 + \text{H.c.}) \\ & + \hbar(\omega + \chi_1\sigma_z^{01} - \chi_2\sigma_z^{12})a^\dagger a \end{aligned} \quad (12)$$

with

$$\sigma_z^{ij} = |j\rangle\langle j| - |i\rangle\langle i|, \quad \chi_i = \frac{g_i^2}{\Delta}, \quad (13)$$

$$\tilde{g} = \frac{g_1 g_2}{\Delta}. \quad (14)$$

By regrouping the terms in Eq. (12), one can check that  $\chi_1$  and  $\chi_2$  are the Stark shifts [2] per photon in the respective JPM levels.

The resulting Hamiltonian describes the system to first order in perturbation theory. We have neglected the terms that contribute to the  $H$  matrix elements as  $\lambda_{1,2}^2 N_{\text{ch}}$  or  $\lambda_1 \lambda_2 N_{\text{ch}}$ , where  $N_{\text{ch}}$  is a characteristic number of photons in the resonator. Hence, Hamiltonian (12) holds if

$$\lambda_{1,2}^2 N_{\text{ch}} \ll 1. \quad (15)$$

A transform is known [38] that *exactly* decouples the first excited state of a three-level atom interacting with a resonator mode. However, it does not accomplish this in the presence of the environment and is hence not useful here.

### B. Interaction picture

It is convenient to move to the interaction picture with a unitary transform  $U_i = \exp(H_0 t/i\hbar)$ , where  $H_0$  is the Hamiltonian of the qubit and the resonator including the parametric interaction terms. This gives rise to

$$H \rightarrow U_i^\dagger H U_i - i\hbar U_i^\dagger \dot{U}_i = \hbar \tilde{g} |2\rangle\langle 0| e^{i\omega t} a^2 + \text{H.c.}, \quad (16)$$

$$r = \chi_1(N - 2\sigma_z^{01}) - \chi_2(1 + N - 2\sigma_z^{12}), \quad N = a^\dagger a. \quad (17)$$

We have used the facts that  $|2\rangle\langle 0| \rightarrow |2\rangle\langle 0| \exp[i\{2\omega - \chi_2(1 + N) + \chi_1 N\}t]$  and  $a^2 \rightarrow a^2 \exp[-2i(\omega + \chi_1 \sigma_z^{01} - \chi_2 \sigma_z^{12})t]$ . The Lindbladian does not change in the interaction picture, as shown in Appendix B.

In the interaction picture, the nondiagonal elements of the density matrix (coherences) do not oscillate with a high frequency. This simplifies the differential equations that govern the matrix elements. More importantly, in the interaction picture decoherence becomes the fastest process. This allows us to make crucial approximations in Sec. IV. Before that, however, we need to check how the Lindbladian changes with the transition to the working frame by the unitary transform  $U$ , which is given in Eq. (10).

### C. Effective Lindbladian

Transition to another frame with the unitary transform  $U$  changes the rates of nonunitary processes. In that frame, a resonator photon gets dressed by the JPM, thus acquiring new channels of tunneling and decay. One needs to find the Lindbladian in our working frame.

While the density matrix transforms by  $\rho \rightarrow U\rho U^\dagger$ , elements of Lindbladians transform as

$$|i\rangle\langle j| \rightarrow U^\dagger |i\rangle\langle j| U, \quad i, j = 0, 1, 2, m. \quad (18)$$

An explicit form of the transformed Lindbladian is given in Appendix C.

### IV. RATE EQUATIONS

Probability of the detector click is given by the occupation of  $|m\rangle$  disregarding the resonator state,

$$P = \sum_{N=0}^{\infty} \rho_{Nm, Nm}. \quad (19)$$

Here and in what follows,

$$\rho_{Mi,Nj} = \langle M | \rho_{ij} | N \rangle, \quad \rho_{ij} = \langle i | \rho | j \rangle, \quad (20)$$

where  $i, j = 0, 1, 2, m$  index the JPM states while  $M$  and  $N$  index the Fock states of the resonator. In Appendix D, we provide the means to write out the exact equations for calculating  $P$ . However, in the regime the device operates well, much simpler equations can be used.

If there are two photons in the resonator, the JPM should fire as fast as possible. After the photons excite the JPM, it should tunnel immediately. More precisely, this should happen much faster than the excitation bounces back coherently to the cavity or the JPM relaxes nonradiatively. In this regime, the JPM decoheres instantaneously; hence, the system state is determined by the probabilities of the excitation to occupy either the cavity or the JPM. In this case we assume that

$$\tilde{\Gamma}_1 + \Gamma_{11} \gg t^{-1}, \quad \tilde{\Gamma}_2 + \Gamma_{22} \gg \tilde{\Gamma}_1, t^{-1}, \quad (21)$$

where  $t$  is the time we observe the system and

$$\tilde{\Gamma}_1 = \gamma_1 + \Gamma_{10}, \quad \tilde{\Gamma}_2 = \gamma_2 + \Gamma_{21}. \quad (22)$$

Also, we assume that

$$\gamma_0 \ll \gamma_1 \ll \gamma_2. \quad (23)$$

We show in Appendix D that, under these conditions, coherences vanish:

$$\rho_{01} \approx \rho_{12} \approx 0. \quad (24)$$

The population of  $|m\rangle$  is then governed by

$$\dot{\rho}_{mm} = \gamma_0 \rho_{00} + \gamma_1 \rho_{11} + \gamma_2 \rho_{22}. \quad (25)$$

Moreover, assuming that  $\rho_{00}$ ,  $\rho_{22}$ , and  $e^{-ir_0 t}$  change slowly, the following rate equations hold:

$$\begin{aligned}\dot{\rho}_{N0,N0} &\approx -B_{NN-2}\rho_{N0,N0} - \gamma_0\rho_{N0,N0} \\ &+ \Gamma_{10}\rho_{N1,N1}, \quad N \geq 2,\end{aligned}\quad (26a)$$

$$\begin{aligned}\dot{\rho}_{N-22,N-22} &\approx B_{NN-2}\rho_{N0,N0} \\ &- \tilde{\Gamma}_2\rho_{N-22,N-22}, \quad N \geq 2,\end{aligned}\quad (26b)$$

$$\dot{\rho}_{N0,N0} \approx -\gamma_0\rho_{N0,N0} + \Gamma_{10}\rho_{N1,N1}, \quad N = 0, 1, \quad (26c)$$

$$\dot{\rho}_{N1,N1} \approx -\tilde{\Gamma}_1\rho_{N1,N1} + \Gamma_{21}\rho_{N2,N2}. \quad (26d)$$

We have defined

$$B_{NN-2} = \frac{4\tilde{g}^2}{\tilde{\Gamma}_2 + \Gamma_{22}}N(N-1), \quad (27)$$

the ratio of absorption of two photons from an  $N$ -photon state. The term  $B_{NN-2}$  is also the stimulated emission rate; however, Eqs. (26) do not contain stimulated emission terms, as the stimulated emission is slow compared to the competing processes. One can figure out from Eqs. (26) that the condition

$$B_{NN-2} \ll \tilde{\Gamma}_2 + \Gamma_{22} \quad (28)$$

should hold, as we have assumed that  $\rho_{00}$  and  $\rho_{22}$  change slowly. Also, as  $e^{-ir_0 t}$  is assumed to change slowly as well, the condition

$$\chi_2 N_{\max} \ll \tilde{\Gamma}_2 + \Gamma_{22} \quad (29)$$

should hold. The fact that  $\chi_2 - \chi_1 \sim \chi_2$  as

$$g_2 \approx \sqrt{2}g_1 \quad (30)$$

was taken into account in the harmonic approximation of the JPM potential. In Eq. (29)  $N_{\max}$  is the highest number of a Fock state such that its occupation is not negligible. Condition (29) is easy to interpret in the laboratory frame. It makes sure that the two-photon transition is not detuned from the Stark-shifted second excited level more than by its linewidth. This interpretation suggests that the condition might be weakened to use the “ $<$ ” inequality sign.

As manifested by Eqs. (26), the dressing does not change the rates of nonunitary processes if the decoherence is fast; this can be explained as follows. Consider  $|10\rangle$  the dressed state of a photon and the ground-state JPM. In terms of the bare states, it is a photon entangled with the excited JPM,  $|10\rangle \approx |10\rangle_b + \lambda_1|01\rangle_b$ . Admixture of the bare excited JPM adds its decay channels to the dressed

state. However, due to the rapid decoherence, the state collapses to a statistical mixture. The addition to the decay rate is then of the order of  $\lambda_1^2$ , which is negligible.

In the next subsections, we calculate the click probabilities for the vacuum, single-photon, and two-photon inputs. In the two-photon mode, a click should be delivered if more than one photon dwells in the resonator; no click should occur in the opposite case. We call clicks that do occur for the vacuum or single-photon input false counts.

### A. Vacuum input

Here we determine the probability of a JPM click in the case when there are no photons in the resonator.

First we determine the initial state of the system. In the laboratory frame, both the JPM and the cavity are in the ground state at the initial instant:

$$|\Psi_b(0)\rangle = |00\rangle. \quad (31)$$

This is also the case in our working frame, i.e.,

$$|\Psi(0)\rangle = U^\dagger|\Psi_b(0)\rangle = |00\rangle, \quad (32)$$

where  $U$  is defined in Eq. (10). Therefore,

$$\rho(0) = |00\rangle\langle 00|. \quad (33)$$

For this case, Eqs. (26), (19), and (25) simplify to

$$P_f = \gamma_0\rho_{00,00} \quad \text{and} \quad \dot{\rho}_{00,00} = -\gamma_0\rho_{00,00}. \quad (34)$$

With the initial conditions given by Eq. (33) and

$$P_f(0) = 0, \quad (35)$$

these equations yield

$$P_f(t) = 1 - e^{-\gamma_0 t} \quad (36)$$

with  $\gamma_0$  the false count rate. The JPM can tunnel even while in the ground state, hence delivering a false count.

### B. One-photon input

Analogously to the previous case, one can determine the initial state. In the laboratory frame

$$|\Psi_b(0)\rangle = |10\rangle, \quad (37)$$

while in the working frame

$$\begin{aligned}|\Psi(0)\rangle &= U^\dagger|\Psi_b(0)\rangle \\ &= |10\rangle + \lambda_1|01\rangle + O(\lambda_1^2) + O(\lambda_2^2),\end{aligned}\quad (38)$$

$$\begin{aligned}\rho(0) &= |10\rangle\langle 10| + \lambda_1|10\rangle\langle 01| + \lambda_1|01\rangle\langle 10| \\ &+ O(\lambda_1^2) + O(\lambda_2^2).\end{aligned}\quad (39)$$

Recall that, in our working frame, there is no interaction with the JPM’s first excited state. However, in this frame,

a bare photon acquires a part of it according to Eq. (38). This may cause a click if the excitation from the first level tunnels.

In the limit of fast decoherence, the dressed initial state coincides with the bare one. Because of Eq. (24), coherences vanish on times (21) we are interested in and

$$\rho(0) \approx |10\rangle\langle 10|. \quad (40)$$

Solving Eqs. (26), (19), and (25) with the initial conditions given by Eqs. (40) and (35) yields

$$P_f(t) = 1 - e^{-\gamma_0 t}. \quad (41)$$

The false count rate for the single-photon input is the same as for the vacuum input. This can be explained as follows. As commented before, the one-photon admixture in Eq. (39) may deliver a click. However, it relies on the system coherence. The coherence dies out momentarily and the admixture decays before the JPM excitation can tunnel. This does not hold in the next order of perturbation theory. Luckily, there is a simple way to estimate the next-order false count rate. This rate provides the limit of applicability of Eq. (41).

Let us calculate the tunneling rate due to the one-photon transition in the next order of perturbation theory. As conditions (21) of the fast decoherence are secured, one can argue in terms of probabilities and transition rates. From Eq. (38), probability of the JPM residing in the first excited state is

$$\langle 1|\rho(0)|1\rangle = \lambda_1^2 + O(\lambda_1^3) + O(\lambda_2^3). \quad (42)$$

According to Eqs. (26), the first excited state tunnels with rate  $\gamma_1$ . Therefore, for the initial state  $\rho(0)$ , the rate of the first-level tunneling is  $\lambda_1^2 \gamma_1$ . Note that Eqs. (26) are obtained up to and including terms of the order of  $\lambda_{1,2}$  only. However, higher-order terms in the equations only give rise to corrections of order beyond  $\lambda_{1,2}^2$  in the rate.

The tunneling rate via the first excited state sets the limit of validity of Eq. (41),

$$t \ll \gamma_1^{-1} \lambda_1^{-2}. \quad (43)$$

For the two-photon input that we consider below, the limit of validity is the same. It can be obtained analogously.

### C. Two-photon input

To determine initial conditions, one applies the same reasoning as for the vacuum and one-photon inputs. This

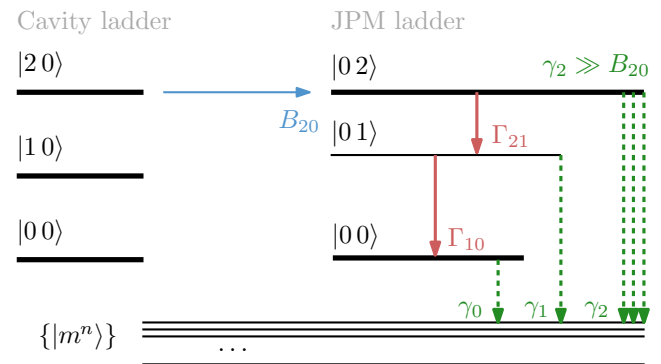


FIG. 4. Two-photon absorption in the limit of fast decoherence and tunneling. The  $\{|m^n\rangle\}$  are the states the JPM can tunnel to.

gives rise to

$$\rho(0) = |20\rangle\langle 20| + \lambda_1|20\rangle\langle 11| + \lambda_1|11\rangle\langle 20|. \quad (44)$$

Because of the fast decoherence, the initial state should be approximated as

$$\rho(0) \approx |20\rangle\langle 20|. \quad (45)$$

This can be shown analogously to the case of one-photon input.

Equations (26), (19), and (25) become

$$\dot{\rho}_{20,20} = -B_{20}\rho_{20,20} - \gamma_0\rho_{20,20}, \quad (46)$$

$$\dot{\rho}_{02,02} = B_{20}\rho_{20,20} - \tilde{\Gamma}_2\rho_{02,02}, \quad (47)$$

$$\dot{\rho}_{01,01} = -\tilde{\Gamma}_1\rho_{01,01} + \Gamma_{21}\rho_{02,02}, \quad (48)$$

$$\dot{\rho}_{00,00} = -\gamma_0\rho_{00,00} + \Gamma_{10}\rho_{01,01}, \quad (49)$$

$$\dot{P}_b = \gamma_0\rho_{20,20} + \gamma_2\rho_{02,02} + \gamma_1\rho_{01,01} + \gamma_0\rho_{00,00}, \quad (50)$$

with

$$B_{20} = 8\tilde{g}^2/(\tilde{\Gamma}_2 + \Gamma_{22}) \quad (51)$$

the two-photon absorption rate. The rate equations are illustrated in Fig. 4. Equations, similar to Eqs. (46)–(50), were obtained in Ref. [8] for the one-photon transition in a two-state JPM well. Compared to the reference equations, our equations lack the stimulated emission terms. This is explained for Eqs. (26). Moreover, the ground level tunneling was not accounted for in Ref. [8].

We solve Eqs. (46)–(50) by carrying out the Laplace transform. The initial conditions are given by Eq. (45) and

$P_b(0) = 0$ . The solution in the Laplace domain is

$$\begin{aligned}\tilde{P}_b(s) &= \frac{\gamma_0 B_{20} \Gamma_{21} \Gamma_{10}}{s(s + \gamma_0)(s + \tilde{\Gamma}_1)\Delta_2} + \frac{\gamma_1 B_{20} \Gamma_{21}}{s(s + \tilde{\Gamma}_1)\Delta_2} \\ &+ \frac{\gamma_0(B_{20} + \tilde{\Gamma}_2) + \gamma_2 B_{20}}{s\Delta_2} + \frac{\gamma_0}{\Delta_2},\end{aligned}\quad (52)$$

where

$$\Delta_2 = (s + \tilde{\Gamma}_2)(s + B_{20} + \gamma_0).\quad (53)$$

Now we find an expression for the click probability in the time domain. It is found by calculating the inverse Laplace transform,

$$P_b(t) = \frac{1}{2\pi i} \int_{\sigma-i\infty}^{\sigma+i\infty} ds e^{st} \tilde{P}_b(s).\quad (54)$$

By carrying out the integrals and doing approximations, one arrives at

$$P_b(t) = 1 - e^{-B_{20}t} - \frac{\Gamma_{21}}{\gamma_2 + \Gamma_{21}} \frac{\Gamma_{10}}{\gamma_1 + \Gamma_{10}} e^{-\gamma_0 t}.\quad (55)$$

We used condition (23) and

$$\gamma_0 \ll B_{20} \ll \tilde{\Gamma}_2,\quad (56)$$

where the last inequality is a more stringent version of condition (28), allowing us to drop the terms proportional to  $B_{20}/\tilde{\Gamma}_2$  and  $\gamma_{0,1}/\tilde{\Gamma}_2$ . These terms are negligibly small in comparison to the second term in the equation. While it turns out that the last term is also small, it decays much slower than the second term. Hence, it is considerable for  $t > 1/B_{20}$ . Equation (55) holds for the times (21) coherence has already vanished.

One can interpret Eq. (55). The second term is the population of state  $|20\rangle$  of the resonator in the two-photon Fock state and the JPM in the ground state. Tunneling from this state is negligible due to Eq. (56). After an excitation transfers from  $|20\rangle$  to  $|02\rangle$  with rate  $B_{20}$ , it tunnels immediately due to condition (28). Hence,  $1 - \exp(-B_{20}t)$  is the tunneling probability for the times before the resonator is depleted. Afterward, the third term in Eq. (55) starts to matter. While absorbing photons, the JPM can also relax to its first excited state  $|1\rangle$ . After all photons are absorbed, the JPM relaxes to  $|1\rangle$  with a small probability  $\Gamma_{21}/(\gamma_2 + \Gamma_{21})$ . From  $|1\rangle$ , the JPM relaxes to the ground state with probability  $\Gamma_{10}/(\gamma_1 + \Gamma_{10})$ . There it is stuck due to the slow ground-state tunneling of rate  $\gamma_0$ , which only becomes substantial for the longer times. While tunneling can also occur from  $|1\rangle$ , this mostly happens while the resonator is not yet depleted and the tunneling from  $|02\rangle$  is ongoing. Because of condition (23), this process is much faster than the tunneling from  $|1\rangle$  and the respective term does not play a role in Eq. (55).

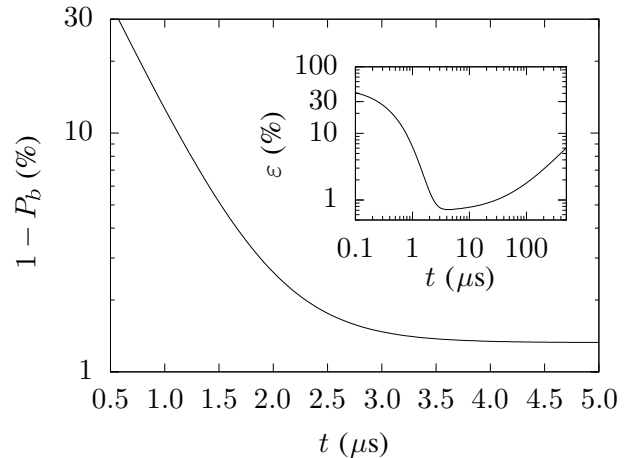


FIG. 5. Probability of missing a two-photon state for a device with the parameters given in Table I. Inset: error in the discrimination of the two-photon state against the states with fewer photons.

#### D. Error probability

One can now calculate the probability of false discrimination between the state with  $N = 2$  photons and the states with  $N = 1$  or  $N = 0$  photons. This error is expressed as

$$\varepsilon = P_{0,1} P_f + P_2 (1 - P_b),\quad (57)$$

where  $P_{0,1} = P_0 + P_1$  and  $P_N$  is a probability of an input state with  $N$  photons to occur. We denote by  $P_b$  the probability of a bright count—i.e., a probability of registering a two-photon state when it dwells in the resonator. We take into account the fact that the probability of a false count  $P_f$  is the same for both  $N = 0$  and  $N = 1$ .

If we know nothing about the resonator state beforehand,  $P_{0,1} = P_2 = \frac{1}{2}$ . Using Eqs. (36) and (41) for  $P_f$  and Eq. (55) for  $P_b$  yields

$$\varepsilon = \frac{1}{2} \left[ 1 + e^{-B_{20}t} + \left( \frac{\Gamma_{21}}{\tilde{\Gamma}_2} \frac{\Gamma_{10}}{\tilde{\Gamma}_1} - 1 \right) e^{-\gamma_0 t} \right].\quad (58)$$

The error probability is plotted in Fig. 5.

With Eq. (58), it is possible to find the minimal error and the optimal waiting time  $t$ . At

$$t \approx \frac{1}{B_{20}} \ln \frac{B_{20}}{\gamma_0}\quad (59)$$

one attains the minimal error

$$\varepsilon \approx \frac{\gamma_0}{2B_{20}} \left( 1 + \ln \frac{B_{20}}{\gamma_0} \right) + \frac{1}{2} \frac{\Gamma_{21}}{\tilde{\Gamma}_2} \frac{\Gamma_{10}}{\tilde{\Gamma}_1}.\quad (60)$$

One can check that the expression is the same if the condition with  $\gamma_0$  in Eq. (56) is not used in obtaining Eq. (55).

TABLE I. Parameters and estimates for the JPM, as well as its performance in the detection of the two-photon state. The junction parameters are from Ref. [39]. The coupling strength  $g_1$  is chosen as described in the text. The bright  $P_b$  [Eq. (55)] and the false  $P_f$  count probabilities [Eqs. (36) and (41)] are given for the optimal waiting time  $t$  [Eq. (59)].

Parameters						Estimated values						Performance			
$C$ (pF)	$I_0$ ( $\mu$ A)	$I/I_0$	$\Gamma_{10}/2\pi$ (kHz)	$\Gamma_{22}/2\pi$ (MHz)	$g_1/2\pi$ (MHz)	$\gamma_0/2\pi$ (Hz)	$\gamma_1/2\pi$ (kHz)	$\gamma_2/2\pi$ (MHz)	$\omega/2\pi$ (GHz)	$\Delta/2\pi$ (MHz)	$B_{20}/2\pi$ (MHz)	$N_{\max}$	$t$ ( $\mu$ s)	$P_f$ (%)	$P_b$ (%)
2	10	0.97987	318	2.1	18.9	37	54	41	8.2	194	0.35	14	4.2	0.1	98.6

### E. More than two photons in the input

For the case when there are  $N > 2$  photons in the cavity, a two-photon transition occurs, leaving  $N - 2$  photons in the cavity. To describe this, one only needs to change the state labels and  $B_{20} \rightarrow B_{NN-2}$  in Eqs. (44)–(60). The bright count probability  $P_b$  improves, as  $B_{NN-2} > B_{20}$  by Eq. (27). By the same reasoning, the error  $\varepsilon$  gets smaller if one needs to discriminate a state with  $N > 2$  photons against the states with one or no photons. Moreover, the error is smaller even if  $N$  breaks condition (15) but requirement (29) still holds. In that case, additional clicks are provided by the single-photon transition and the subsequent tunneling from the first level.

### V. DISTINGUISHING A MULTIPHOTON STATE

In this section, example parameters for the JPM in the two-photon mode are provided. For these parameters, we estimate the probabilities of bright and false counts, the time to distinguish a multiphoton state, and the probability of false discrimination.

First let us summarize the requirements for our JPM to work as described above. The energy of the junction plasma oscillations should much exceed that of a thermal excitation,  $\hbar\omega_p \gg k_B T$ , where  $T$  is the temperature of the JPM environment. On the other hand, we do not want to spur quasiparticles while exciting the JPM. Hence,

$$\omega_p \ll \Delta_{\text{gap}}, \quad (61)$$

where  $\Delta_{\text{gap}}$  is the superconductor gap. Furthermore, the effective Lindbladian (C1) we have used is correct if conditions (15) and (43) hold. Finally, we have required the JPM to decohere fast by conditions (21) and (28)–(29).

It is convenient to introduce the Josephson energy

$$E_J = \frac{I_0 \Phi_0}{2\pi} \quad (62)$$

and the capacitive energy

$$E_C = \frac{e^2}{2C}. \quad (63)$$

The ratio

$$\beta = I/I_0 \quad (64)$$

is given in Table I. For this ratio, three levels fit in the well.

One needs to know the position of the levels in the well. To this end, we expand the potential around the well minimum up to the cubic terms:

$$\frac{W}{E_J} \approx \frac{\sqrt{1 - \beta^2}}{2} \delta^2 - \frac{\beta}{6} \delta^3. \quad (65)$$

Here  $\delta = 2\pi\Phi/\Phi_0 - \phi_{\min}$  is the dimensionless flux with respect to the well minimum at  $\phi_{\min} = \arcsin\beta$ . To determine the level structure correctly, the cubic approximation should be accurate in the region up to the barrier maximum at  $\delta_{\max} = 2 \cot \phi_{\min}$ . For a weak anharmonicity, one can calculate the position of the levels using second-order perturbation theory [40,41]. It is useful to define

$$n_0 = \frac{(1 - \beta^2)^{5/4}}{3\beta^2} \sqrt{\frac{E_J}{2E_C}}, \quad (66)$$

the barrier height, in units of

$$\omega_p = \frac{1}{\hbar} \sqrt{8E_J E_C} (1 - \beta^2)^{1/4}, \quad (67)$$

the level separation in the harmonic approximation. Equations (66) and (67) coincide with those given in Ref. [41]. The transition frequency from the ground to the first excited state is  $\omega_{10} = \omega_p (1 - 5/36n_0)$ . The transition frequency to the second excited state is  $\omega_{20} = \omega_p (2 - 5/12n_0)$  [42]. We aim to detect photons of frequency

$$\omega = \omega_{02}/2. \quad (68)$$

This photon is detuned from the  $0 \rightarrow 1$  transition by

$$\Delta = \omega_{10} - \omega = \frac{5}{72} \frac{\omega_p}{n_0}. \quad (69)$$

We provide the value of  $\Delta$  in Table I.

Knowledge of  $\Delta$  allows one to set  $g_1$  and  $g_2$ . One can use criterion (15) for that. To be sure that no clicks are delivered when there is a single photon in the resonator, Eq. (15) should hold for  $N_{\text{ch}} = 1$ . This requirement does not matter for larger photon numbers—by reasoning similar to that given at the end of Sec. IV D. So, we choose

$\lambda_2 = 0.1$ , which fulfills one of the requirements in Eq. (15) for  $N_{\text{ch}} = 1$ . By virtue of Eq. (30), the part of condition (15) with  $\lambda_1$  [see Eq. (11)] holds automatically. From the definitions of  $\lambda_1$  and  $\lambda_2$  given in Eq. (11) and relationship (30), one obtains

$$g_2 = \lambda_2 \Delta, \quad g_1 = \lambda_2 \Delta / \sqrt{2}. \quad (70)$$

One also needs to make sure that condition (29) holds. This yields the biggest photon number  $N_{\text{max}}$  that can be distinguished from the single-photon and vacuum states. Its value is given in Table I.

Let us calculate the rate  $B_{20}$  of the two-photon absorption. It follows from Eqs. (51), (14), (70), and (11) that

$$B_{20} \approx 4\lambda_2^4 \Delta^2 / (\tilde{\Gamma}_2 + \Gamma_{22}). \quad (71)$$

Assuming flat density of states of the thermal reservoir, one can estimate in the harmonic approximation that

$$\Gamma_{21} \approx 2\Gamma_{10}. \quad (72)$$

Tunneling rates  $\gamma_0$ ,  $\gamma_1$ , and  $\gamma_2$  are calculated with the WKB method [40] and are given in Table I. We used the expression [41]

$$\gamma_n = \frac{\omega_n}{n! \sqrt{2\pi}} \left( \frac{n+1/2}{e} \right)^{n+1/2} \exp \left( -\frac{2S}{\hbar} \right) \quad (73)$$

for the tunneling rate. The integral in the action  $S = \int_{\Phi_1}^{\Phi_2} d\Phi \sqrt{2C(W - \hbar\omega_n)}$  is carried out numerically for the exact potential  $W$  given by Eq. (3). The  $n$ th level eigenfrequencies  $\omega_n$  and the barrier boundaries  $\Phi_1$  and  $\Phi_2$  are determined using the cubic approximation. With all the necessary quantities obtained, one can calculate  $B_{20}$ . Its value is provided in Table I.

Now one can estimate the JPM performance. The error (58) and the probability to miss a two-photon state  $1 - P_b$  [see Eq. (55)] are shown in Fig. 5. The dominant contribution to the false counts at the optimal counting time (59) is due to the ground level tunneling as given by Eqs. (36) and (41). The false count probability is given in Table I. Transitions to the first excited state  $|1\rangle$  in the second-order perturbation theory in  $\lambda_{1,2}$  contribute as well. However, one can check that, by criterion (43), their effect is still vanishing for the relevant times. Also,  $|1\rangle$  could be excited by an off-resonant single photon due to the level widening. However, this is highly improbable, as

$$\tilde{\Gamma}_1 + \Gamma_{11} \ll \Delta. \quad (74)$$

## VI. COUNTING TO TWO

A two-step procedure (see Fig. 1 and Sec. I) is to be performed to count photons to two. To switch from the

two-photon mode to the single-photon mode, the bias current  $I$  [see Fig. 2 and Hamiltonian (3)] is changed so that the JPM possesses two metastable states instead of three. Here we estimate the error in discrimination between the vacuum input state, a one-photon state, and a multiphoton state. The total time of the discrimination is estimated as well.

The full time to count to two is approximately the same as the time to distinguish a multiphoton state versus the vacuum or single-photon state. Additional time consists of the time to switch to the single-photon mode and the time to discriminate the vacuum state. To spur no excitations in the JPM, the switching should be much slower than the inverse transition frequencies. For the parameters in Table I, the switching can be as fast as 10 ns. Now let us compare the waiting times. The time to discriminate a multiphoton state is determined by  $B_{20}$ , as it follows from Eq. (55). The time to discriminate the vacuum is set by  $\gamma_1$  in the two-state configuration with  $B_{10}$  the single-photon absorption rate. The latter can be calculated analogously to the two-photon absorption rate (51). This yields  $B_{10} = 4g_1^2 / (\tilde{\Gamma}_1 + \Gamma_{11})$ . With Eq. (14) one has

$$\frac{B_{20}}{B_{10}} = 2\lambda_2^2 \frac{\tilde{\Gamma}_1 + \Gamma_{11}}{\tilde{\Gamma}_2 + \Gamma_{22}} \approx \lambda_2^2. \quad (75)$$

Equation (72) and the fact that decay is much faster than the pure decoherence were used in obtaining the last equality in Eq. (75). The WKB estimate for the tunneling rate from the excited state gives

$$\gamma_1 \approx 2\pi 19 \text{ MHz}. \quad (76)$$

We choose  $I/I_0 = 0.98473$  to fit two levels in the well. By Eq. (76), as well as by the value of  $B_{20}$  from Table I and Eq. (75), discrimination of the vacuum state is much faster than that of a multiphoton state.

Now we find the probability to incorrectly determine the number of input photons. Let  $P_b^{0/1}$  denote the probability to correctly identify a single-photon state in the second stage;  $P_b$  denotes that in the first stage as before. The probability of error in the two-step discrimination is then

$$\epsilon^{0/1/2} = P_0 P_f + P_1 [P_f + (1 - P_f)(1 - P_b^{0/1})] + P_2 (1 - P_b). \quad (77)$$

We take into account the fact that the false count probability is negligible for the second stage, as compared to the false count probability  $P_f$  in the first stage. This is due to the detection time in the second stage being much smaller than that in the first stage. We assume that nothing is known about the input and  $P_0 = P_1 = P_2 = \frac{1}{3}$ . One can

rewrite Eq. (77) in a more convenient form:

$$\varepsilon^{0/1/2} = \frac{1}{3}[P_f(1 + P_b^{0/1}) + 1 - P_b^{0/1} + 1 - P_b]. \quad (78)$$

To compute  $\varepsilon^{0/1/2}$ , one needs to estimate  $P_b^{0/1}$ . For the optimal counting time, a photon is most probably absorbed by the JPM. However, this does not necessarily give a click: a photon could get stuck in the ground state due to the JPM relaxation with a probability  $\Gamma_{10}/(\Gamma_{10} + \gamma_1)$ . Therefore,

$$P_b^{0/1} \approx \gamma_1/(\Gamma_{10} + \gamma_1) \approx 98.3\%, \quad (79)$$

where estimate (76) was used. Equation (79) was also given in Ref. [43]. With estimate (79) and the values from Table I, one obtains

$$\varepsilon^{0/1/2} \approx 1.1\%. \quad (80)$$

The optimal time can be chosen to minimize the full counting error (78) instead of that in the discrimination of a multiphoton state [see Eq. (58)]. However, this does not improve the full error substantially.

## VII. DISCUSSION

We have proposed a detector of microwave photons with limited photon-number resolution. Realistic parameters have been provided that allow distinguishing between the vacuum, single-photon, and multiphoton states in 4.2  $\mu$ s with a 1.1% error probability. The most time-consuming part in the device operation is the discrimination of a multiphoton state versus the single-photon or vacuum state. The speed of this step is limited by the two-photon absorption rate, which in turn is set by the coupling strength of the JPM to the cavity. To avoid single-photon transitions, the coupling should be much weaker than the JPM anharmonicity. A larger anharmonicity can lead to faster detection. Moreover, faster detection decreases the false count probability  $P_f$ . The probability to count photons incorrectly is determined by  $P_f$  and the probabilities to miss the multi- and single-photon states. As for the probabilities to miss photons, they are determined by branching ratios between the excited state tunneling and relaxation.

For the proposed parameters, the 8.2 GHz photons are detected. The frequency can be chosen at the design stage in the range from 1 to 20 GHz. The upper limit on the frequency is set by the superconducting gap of aluminum, which is about 82 GHz, and condition (61). As for the lower limit, it is determined by requirement (74), relationship (69) between the plasma frequency and the anharmonicity, and an estimate for the decoherence of the JPM's first excited state, which is about 1 MHz.

Two possibilities for development of the detector are worth mentioning. First, one can use it for the detection

of itinerant photons. One option is to attach the resonator to a waveguide; it will function as a capture cavity from Ref. [7]. Another option is to attach a waveguide directly. This introduces reflection losses; to minimize them, the detector should be matched to its input [44]. Secondly, one can envision a detector that counts photons up to  $N$ . This device might use an  $N$ -photon transition through  $N - 2$  auxiliary levels at the first stage to discriminate the states with  $N$  or more photons. Afterward, it can be sequentially tuned to discriminate the states with  $N - 1$ ,  $N - 2$ , and down to 1 photon.

## ACKNOWLEDGMENTS

The work of A.S. is supported by a DAAD scholarship (2016). We thank Robert McDermott for useful comments on the manuscript.

## APPENDIX A: DERIVATION OF THE CIRCUIT HAMILTONIAN

The Lagrangian of the system is given by

$$\mathcal{L} = \mathcal{L}_{\text{JPM}} + \mathcal{L}_r + \mathcal{L}_c, \quad (\text{A1})$$

$$\mathcal{L}_{\text{JPM}} = \frac{C\dot{\Phi}^2}{2} + E_J \cos 2\pi \frac{\Phi}{\Phi_0} + I\Phi, \quad (\text{A2})$$

$$\mathcal{L}_c = \frac{C'(\dot{\Phi} - \dot{\Phi}_r)^2}{2}, \quad (\text{A3})$$

$$\mathcal{L}_r = \frac{C_r\dot{\Phi}_r^2}{2} - \frac{\Phi_r^2}{2L_r}. \quad (\text{A4})$$

Here  $E_J$  is defined by Eq. (62).

Generalized momenta are

$$Q = \partial \mathcal{L} / \partial \dot{\Phi} = (C + C')\dot{\Phi} - C'\dot{\Phi}_r, \quad (\text{A5})$$

$$Q_r = \partial \mathcal{L} / \partial \dot{\Phi}_r = -C'\dot{\Phi} + (C_r + C')\dot{\Phi}_r. \quad (\text{A6})$$

The system Hamiltonian is given by the Legendre transform,

$$H = Q\dot{\Phi} + Q_r\dot{\Phi}_r - \mathcal{L}. \quad (\text{A7})$$

One needs to find the kinetic energy part  $T$  of  $H$ . It is a quadratic form in  $Q$  and  $Q_r$ ,

$$T = \frac{1}{2} \frac{\partial^2 H}{\partial Q^2} Q^2 + \frac{1}{2} \frac{\partial^2 H}{\partial Q_r^2} Q_r^2 + \frac{\partial^2 H}{\partial Q \partial Q_r} QQ_r \\ + \left. \frac{\partial H}{\partial Q} \right|_{Q,Q_r=0} Q + \left. \frac{\partial H}{\partial Q_r} \right|_{Q,Q_r=0} Q_r. \quad (\text{A8})$$

We used the fact that the potential energy, which composes the rest of  $H$ , does not depend on the momenta. Differentiating Eq. (A7) and using the expressions for generalized

momenta, Eqs. (A5)–(A6), gives

$$\partial^2 H / \partial Q^2 = \partial \dot{\Phi} / \partial Q \quad (\text{A9})$$

and  $\partial H / \partial Q|_{Q,Q_r=0} = 0$ . Other coefficients are given by similar formulas. One then determines the renormalized capacitances

$$\tilde{C} = \frac{C + C'(1 + C/C_r)}{1 + C'/C_r}, \quad \tilde{C}_r = \frac{C_r + C'(1 + C_r/C)}{1 + C'/C}, \quad (\text{A10})$$

$$\tilde{C}' = \left( \frac{1'}{C} + \frac{1}{C} + \frac{1}{C_r} \right)^{-1}, \quad (\text{A11})$$

in Hamiltonians (1)–(4).

## APPENDIX B: LINDBLADIAN DOES NOT CHANGE IN THE INTERACTION PICTURE

The density matrix transforms as  $\rho \rightarrow U\rho U^\dagger$ . To leave the Lindblad equation (7) invariant, the Lindbladian becomes

$$L\rho \rightarrow L\rho - \dot{U}\rho U^\dagger - U\rho \dot{U}^\dagger. \quad (\text{B1})$$

With  $U = \exp(H_0 t / i\hbar)$ , the Lindbladian stays the same.

## APPENDIX C: DRESSED LINDBLAD EQUATION

Here we write out the explicit form of the first-order corrections in the Lindbladian in our working frame.

On applying the transform  $U$  (10), Lindbladian (7) becomes

$$L \rightarrow L + L^{(1)}, \quad (\text{C1})$$

where  $L^{(1)}$  is first order in  $\lambda_1$  and  $\lambda_2$ . It can be given in terms of its matrix elements:

$$\begin{aligned} \langle 0 | L^{(1)} \rho | 0 \rangle &= \lambda_2 \Gamma_{10} a^\dagger \langle 2 | \rho | 1 \rangle - \frac{1}{2} \lambda_1 (\gamma_1 - \gamma_0 + \Gamma_{11} + \Gamma_{10}) a^\dagger \langle 1 | \rho | 0 \rangle + \lambda_1 \Gamma_{10} a \langle 0 | \rho | 1 \rangle + \text{c.c.}, \\ \langle 1 | L^{(1)} \rho | 1 \rangle &= \frac{1}{2} \lambda_2 (\gamma_2 - \gamma_1 + \Gamma_{22} + \Gamma_{21} + \Gamma_{11} - \Gamma_{10}) a^\dagger \langle 2 | \rho | 1 \rangle - \lambda_2 \Gamma_{21} a \langle 1 | \rho | 2 \rangle \\ &\quad - \frac{1}{2} \lambda_1 (\gamma_1 - \gamma_0 - \Gamma_{11} + \Gamma_{10}) a \langle 0 | \rho | 1 \rangle + \text{c.c.}, \\ \langle 2 | L^{(1)} \rho | 2 \rangle &= \frac{1}{2} \lambda_2 (\gamma_2 - \gamma_1 - \Gamma_{22} + \Gamma_{21} - \Gamma_{11} - \Gamma_{10}) a \langle 1 | \rho | 2 \rangle + \text{c.c.}, \\ \langle m | L^{(1)} \rho | m \rangle &= \lambda_2 \gamma_1 a^\dagger \langle 2 | \rho | 1 \rangle - \lambda_1 \gamma_0 a^\dagger \langle 1 | \rho | 0 \rangle - \lambda_2 \gamma_2 a \langle 1 | \rho | 2 \rangle + \lambda_1 \gamma_1 a \langle 0 | \rho | 1 \rangle + \text{c.c.}, \\ \langle 0 | L^{(1)} \rho | 1 \rangle &= \lambda_1 \Gamma_{21} a^\dagger \langle 2 | \rho | 2 \rangle - \frac{1}{2} \lambda_1 (\gamma_1 - \gamma_0 - \Gamma_{11} + \Gamma_{10}) a^\dagger \langle 1 | \rho | 1 \rangle \\ &\quad - \lambda_1 \Gamma_{10} \langle 1 | \rho a^\dagger | 1 \rangle - \frac{1}{2} \lambda_1 (\gamma_1 - \gamma_0 + \Gamma_{11} + \Gamma_{10}) \langle 0 | \rho a^\dagger | 0 \rangle \\ &\quad + \frac{1}{2} \lambda_2 (\gamma_2 - \gamma_1 + \Gamma_{22} + \Gamma_{21} - \Gamma_{11} - \Gamma_{10}) \langle 0 | \rho a | 2 \rangle, \\ \langle 1 | L^{(1)} \rho | 2 \rangle &= \frac{1}{2} \lambda_2 (\gamma_2 - \gamma_1 - \Gamma_{22} + \Gamma_{21} - \Gamma_{11} - \Gamma_{10}) a^\dagger \langle 2 | \rho | 2 \rangle - \frac{1}{2} \lambda_1 (\gamma_1 - \gamma_0 + \Gamma_{11} + \Gamma_{10}) a \langle 0 | \rho | 2 \rangle \\ &\quad + \lambda_2 \Gamma_{21} \langle 2 | \rho a^\dagger | 2 \rangle + \frac{1}{2} \lambda_2 (\gamma_2 - \gamma_1 + \Gamma_{22} + \Gamma_{21} + \Gamma_{11} - \Gamma_{10}) \langle 1 | \rho a^\dagger | 1 \rangle, \\ \langle 0 | L^{(1)} \rho | 2 \rangle &= \frac{1}{2} \lambda_2 (\gamma_2 - \gamma_1 + \Gamma_{22} + \Gamma_{21} - \Gamma_{11} - \Gamma_{10}) \langle 0 | \rho a^\dagger | 1 \rangle - \frac{1}{2} \lambda_1 (\gamma_1 - \gamma_0 + \Gamma_{11} + \Gamma_{10}) a^\dagger \langle 1 | \rho | 2 \rangle, \\ \langle m | L^{(1)} \rho | 0 \rangle &= -\frac{1}{2} \lambda_1 (\gamma_1 - \gamma_0 + \Gamma_{11} + \Gamma_{10}) \langle m | \rho a | 1 \rangle, \\ \langle m | L^{(1)} \rho | 1 \rangle &= \frac{1}{2} \lambda_2 (\gamma_2 - \gamma_1 + \Gamma_{22} + \Gamma_{21} - \Gamma_{11} - \Gamma_{10}) \langle m | \rho a | 2 \rangle - \frac{1}{2} \lambda_1 (\gamma_1 - \gamma_0 + \Gamma_{11} + \Gamma_{10}) \langle m | \rho a^\dagger | 0 \rangle, \\ \langle m | L^{(1)} \rho | 2 \rangle &= \frac{1}{2} \lambda_2 (\gamma_2 - \gamma_1 + \Gamma_{22} + \Gamma_{21} - \Gamma_{11} - \Gamma_{10}) \langle m | \rho a^\dagger | 1 \rangle. \end{aligned}$$

## APPENDIX D: DERIVATION OF THE RATE EQUATIONS

### 1. Exact equations to find the probability of the detector click

First we write out the exact equations that allow us to calculate the probability of the detector click (19).

We start with providing the equation for  $\rho_{mm}$ . Projecting the dressed Lindbladian (C1) on  $|m\rangle$  gives

$$\begin{aligned} \dot{\rho}_{mm} &= \gamma_0 \rho_{00} + \gamma_1 \rho_{11} + \gamma_2 \rho_{22} \\ &\quad + (\gamma_1 \lambda_2 \rho_{12} a - \gamma_0 \lambda_1 \rho_{01} a \\ &\quad - \gamma_2 \lambda_2 a \rho_{12} + \gamma_1 \lambda_1 a \rho_{01} + \text{H.c.}). \end{aligned} \quad (\text{D1})$$

The equation is given up to and including terms of order  $\lambda_1$  and  $\lambda_2$ .

To complete the equation, one needs equations for  $\dot{\rho}_{00}$ ,  $\dot{\rho}_{11}$ , and  $\dot{\rho}_{22}$  with the same accuracy. For  $\dot{\rho}_{12}$  and  $\dot{\rho}_{01}$ , a zeroth approximation in  $\lambda_1$  and  $\lambda_2$  would suffice. It is convenient to use the reduced  $r$  (17),

$$r_0 = \langle 0|r|0 \rangle, \quad (\text{D2})$$

which considers the JPM in the ground state  $|0\rangle$  and acts solely on the resonator. Equations (C1) and (16)–(17) yield

$$\begin{aligned} \dot{\rho}_{00} = & (i\tilde{g}\rho_{02}e^{ir_0t}a^2 + \text{H.c.}) - \gamma_0\rho_{00} + \Gamma_{10}\rho_{11} \\ & + \langle 0|L^{(1)}|0 \rangle, \end{aligned} \quad (\text{D3})$$

$$\dot{\rho}_{11} = -(\gamma_1 + \Gamma_{10})\rho_{11} + \Gamma_{21}\rho_{22} + \langle 1|L^{(1)}|1 \rangle, \quad (\text{D4})$$

$$\begin{aligned} \dot{\rho}_{22} = & (-i\tilde{g}e^{ir_0t}a^2\rho_{02} + \text{H.c.}) - (\gamma_2 + \Gamma_{21})\rho_{22} \\ & + \langle 2|L^{(1)}|2 \rangle, \end{aligned} \quad (\text{D5})$$

to first order in  $\lambda_1$  and  $\lambda_2$ . Next we express

$$\dot{\rho}_{01} = -i\tilde{g}a^{\dagger 2}e^{-ir_0t}\rho_{21} - \frac{1}{2}d_{01}\rho_{01} + O(\lambda_1 + \lambda_2), \quad (\text{D6})$$

$$\dot{\rho}_{12} = i\tilde{g}\rho_{10}a^{\dagger 2}e^{-ir_0t} - \frac{1}{2}d_{12}\rho_{12} + O(\lambda_1 + \lambda_2), \quad (\text{D7})$$

in terms of  $\rho_{00}$ ,  $\rho_{11}$ , and  $\rho_{22}$ , as well as

$$\begin{aligned} \dot{\rho}_{02} = & i\tilde{g}\rho_{00}a^{\dagger 2}e^{-ir_0t} - i\tilde{g}a^{\dagger 2}e^{-ir_0t}\rho_{22} \\ & - \frac{1}{2}d_{02}\rho_{02} + \langle 0|L^{(1)}|2 \rangle + O(\lambda_1^2 + \lambda_2^2 + \lambda_1\lambda_2), \end{aligned} \quad (\text{D8})$$

where

$$d_{01} = \gamma_0 + \gamma_1 + \Gamma_{10} + \Gamma_{11}, \quad (\text{D9})$$

$$d_{12} = \gamma_1 + \gamma_2 + \Gamma_{10} + \Gamma_{21} + \Gamma_{22}, \quad (\text{D10})$$

$$d_{02} = \gamma_0 + \gamma_2 + \Gamma_{21} + \Gamma_{22}, \quad (\text{D11})$$

are the full decoherence rates of the  $0 \rightarrow 1$ ,  $1 \rightarrow 2$ , and  $0 \rightarrow 2$  transitions, respectively. Because of the forms of Eqs. (D3) and (D5), we have calculated  $\dot{\rho}_{02}$  to first order in  $\lambda_1$  and  $\lambda_2$ .

It is not hard to write out a full set of equations to calculate  $\rho_{mm}$  and  $P$ . To this end, one uses the expressions for the  $L^{(1)}$  matrix elements from Appendix C and projects Eqs. (D1) and (D3)–(D8) on the photon-number states.

## 2. Fast decoherence

Here we obtain the rate equations for the case of fast decoherence. By Eqs. (21) and (23), Eqs. (D9) and (D10) yield  $d_{01} \approx \tilde{\Gamma}_1 + \Gamma_{11}$  and  $d_{12} \approx \tilde{\Gamma}_2 + \Gamma_{22}$ . Moreover, at time  $t$ , coherences have already died out: Eq. (24) follows from the form of Eqs. (D6)–(D7) and conditions (21). Equation (D1) then simplifies to Eq. (25).

One can show that the system is then governed by rate equations. First we express  $\rho_{02}$  in terms of the probabilities  $\rho_{00}$  and  $\rho_{22}$ . The formal solution of Eq. (D8) reads

$$\begin{aligned} \rho_{02}(t) \approx & \rho_{02}(0)e^{-(\tilde{\Gamma}_2 + \Gamma_{22})t/2} \\ & + i\tilde{g} \int_0^t dt' e^{-(\tilde{\Gamma}_2 + \Gamma_{22})(t-t')/2} \\ & \times [\rho_{00}a^{\dagger 2}e^{-ir_0t'} - a^{\dagger 2}e^{-ir_0t'}\rho_{22}e^{\tilde{\Gamma}_2 t'}e^{-\tilde{\Gamma}_2 t'}]. \end{aligned} \quad (\text{D12})$$

The first term on the right-hand side vanishes due to Eqs. (21). Now we make an approximation similar to the Weisskopf-Wigner approximation: we assume that  $a^{\dagger}(t')$ ,  $e^{-ir_0t'}$ ,  $\rho_{00}(t')$ , and  $\rho_{22}(t')e^{\tilde{\Gamma}_2 t'}$  change slowly in comparison to the rate  $\tilde{\Gamma}_2$ . Removing these terms from the integral allows one to perform the integration, which yields

$$\rho_{02}(t) \approx i \frac{2\tilde{g}}{\tilde{\Gamma}_2 + \Gamma_{22}} \rho_{00}a^{\dagger 2}e^{-ir_0t}. \quad (\text{D13})$$

Substituting this into Eqs. (D3)–(D5) and projecting them on the resonator Fock states gives Eqs. (26). We also used the fact that the matrix elements  $\langle i|L^{(1)}|i \rangle \approx 0$  for  $i = 0, 1, 2$  due to Eq. (24).

- 
- [1] J. Q. You and F. Nori, Atomic physics and quantum optics using superconducting circuits, *Nature* **474**, 589 (2011).
  - [2] A. Blais, R.-S. Huang, A. Wallraff, S. M. Girvin, and R. J. Schoelkopf, Cavity quantum electrodynamics for superconducting electrical circuits: An architecture for quantum computation, *Phys. Rev. A* **69**, 062320 (2004).
  - [3] Y.-F. Chen, D. Hover, S. Sendelbach, L. Maurer, S. T. Merkel, E. J. Pritchett, F. K. Wilhelm, and R. McDermott, Microwave Photon Counter Based on Josephson Junctions, *Phys. Rev. Lett.* **107**, 217401 (2011).
  - [4] P. Forn-Díaz, L. Lamata, E. Rico, J. Kono, and E. Solano, Ultrastrong coupling regimes of light-matter interaction, *Rev. Mod. Phys.* **91**, 025005 (2019).
  - [5] A. Frisk Kockum, A. Miranowicz, S. De Liberato, S. Savasta, and F. Nori, Ultrastrong coupling between light and matter, *Nat. Rev. Phys.* **1**, 19 (2019).
  - [6] F. Wilhelm, R. Steinwandt, B. Langenberg, P. Liebermann, A. Messinger, and P. Schuhmacher, *Entwicklungsstand Quantencomputer*, Tech. Rep. (Federal Office for Information Security, Bonn, Germany, 2018) in English.
  - [7] A. Opremcak, I. V. Pechenezhskiy, C. Howington, B. G. Christensen, M. A. Beck, E. Leonard, J. Suttle, C. Wilen,

- K. N. Nesterov, G. J. Ribeill, T. Thorbeck, F. Schlenker, M. G. Vavilov, B. L. T. Plourde, and R. McDermott, Measurement of a superconducting qubit with a microwave photon counter, *Science* **361**, 1239 (2018).
- [8] L. C. G. Govia, E. J. Pritchett, S. T. Merkel, D. Pineau, and F. K. Wilhelm, Theory of Josephson photomultipliers: Optimal working conditions and back action, *Phys. Rev. A* **86**, 032311 (2012).
- [9] G. Oelsner, C. K. Andersen, M. Rehák, M. Schmelz, S. Anders, M. Grajcar, U. Hübner, K. Mølmer, and E. Il'ichev, Detection of Weak Microwave Fields with an Underdamped Josephson Junction, *Phys. Rev. Appl.* **7**, 014012 (2017).
- [10] G. Oelsner and E. Il'ichev, Switching dynamics of an underdamped Josephson junction coupled to a microwave cavity, *J. Low Temp. Phys.* **192**, 169 (2018).
- [11] K. Inomata, Z. Lin, K. Koshino, W. D. Oliver, J.-S. Tsai, T. Yamamoto, and Y. Nakamura, Single microwave-photon detector using an artificial I-type three-level system, *Nat. Commun.* **7**, 12303 (2016).
- [12] J.-C. Besse, S. Gasparinetti, M. C. Collodo, T. Walter, P. Kurpiers, M. Pechal, C. Eichler, and A. Wallraff, Single-Shot Quantum Nondemolition Detection of Individual Itinerant Microwave Photons, *Phys. Rev. X* **8**, 021003 (2018).
- [13] J.-C. Besse, S. Gasparinetti, M. C. Collodo, T. Walter, A. Remm, J. Krause, C. Eichler, and A. Wallraff, Parity Detection of Propagating Microwave Fields, *Phys. Rev. X* **10**, 011046 (2020).
- [14] B. R. Johnson, M. D. Reed, A. A. Houck, D. I. Schuster, L. S. Bishop, E. Ginossar, J. M. Gambetta, L. DiCarlo, L. Frunzio, S. M. Girvin, and R. J. Schoelkopf, Quantum non-demolition detection of single microwave photons in a circuit, *Nat. Phys.* **6**, 663 (2010).
- [15] R. Dassonneville, R. Assouly, T. Peronnin, P. Rouchon, and B. Huard, Number-resolved photocounter for propagating microwave mode, arXiv:2004.05114 (2020).
- [16] R. Lescanne, S. Deléglise, E. Albertinale, U. Réglade, T. Capelle, E. Ivanov, T. Jacqmin, Z. Leghtas, and E. Flurin, Irreversible Qubit-Photon Coupling for the Detection of Itinerant Microwave Photons, *Phys. Rev. X* **10**, 021038 (2020).
- [17] B. Peropadre, G. Romero, G. Johansson, C. M. Wilson, E. Solano, and J. J. García-Ripoll, Approaching perfect microwave photodetection in circuit qed, *Phys. Rev. A* **84**, 063834 (2011).
- [18] B. Fan, G. Johansson, J. Combes, G. J. Milburn, and T. M. Stace, Nonabsorbing high-efficiency counter for itinerant microwave photons, *Phys. Rev. B* **90**, 035132 (2014).
- [19] A. L. Grimsmo, B. Royer, J. M. Kreikebaum, Y. Ye, K. O'Brien, I. Siddiqi, and A. Blais, Quantum metamaterial for nondestructive microwave photon counting, arXiv:2005.06483 (2020).
- [20] I. Iakoupov, Y. Matsuzaki, W. J. Munro, and S. Saito, Sequential nonabsorbing microwave single-photon detector, *Phys. Rev. Res.* **2**, 033238 (2020).
- [21] A. Roy and M. Devoret, Quantum-limited parametric amplification with Josephson circuits in the regime of pump depletion, *Phys. Rev. B* **98**, 045405 (2018).
- [22] T. Walter, P. Kurpiers, S. Gasparinetti, P. Magnard, A. Potočnik, Y. Salathé, M. Pechal, M. Mondal, M. Oppliger, C. Eichler, and A. Wallraff, Rapid High-Fidelity Single-Shot Dispersive Readout of Superconducting Qubits, *Phys. Rev. Appl.* **7**, 054020 (2017).
- [23] R. McDermott, M. G. Vavilov, B. L. T. Plourde, F. K. Wilhelm, P. J. Liebermann, O. A. Mukhanov, and T. A. Ohki, Quantum-classical interface based on single flux quantum digital logic, *Quantum Sci. Technol.* **3**, 024004 (2018).
- [24] M. P. V. Stenberg, K. Pack, and F. K. Wilhelm, Adaptive identification of coherent states, *Phys. Rev. A* **92**, 063852 (2015).
- [25] L. C. G. Govia, E. J. Pritchett, C. Xu, B. L. T. Plourde, M. G. Vavilov, F. K. Wilhelm, and R. McDermott, High-fidelity qubit measurement with a microwave-photon counter, *Phys. Rev. A* **90**, 062307 (2014).
- [26] A. Opremcak, C. Liu, C. Wilen, K. Okubo, B. Christensen, D. Sank, T. White, A. Vainsencher, M. Giustina, A. Megrant *et al.*, High-fidelity measurement of a superconducting qubit using an on-chip microwave photon counter, arXiv:2008.02346 (2020).
- [27] A. Sokolov, Optimal conditions for high-fidelity dispersive readout of a qubit with a photon-number-resolving detector, *Phys. Rev. A* **93**, 032323 (2016).
- [28] C. Wittmann, U. L. Andersen, M. Takeoka, D. Sych, and G. Leuchs, Discrimination of binary coherent states using a homodyne detector and a photon number resolving detector, *Phys. Rev. A* **81**, 062338 (2010).
- [29] R. H. Hadfield, M. J. Stevens, S. S. Gruber, A. J. Miller, R. E. Schwall, R. P. Mirin, and S. W. Nam, Single photon source characterization with a superconducting single photon detector, *Opt. Express* **13**, 10846 (2005).
- [30] Z. H. Peng, S. E. de Graaf, J. S. Tsai, and O. V. Astafiev, Tuneable on-demand single-photon source in the microwave range, *Nat. Commun.* **7**, 12588 (2016).
- [31] P. Forn-Díaz, C. W. Warren, C. W. S. Chang, A. M. Vadhiraj, and C. M. Wilson, On-Demand Microwave Generator of Shaped Single Photons, *Phys. Rev. Appl.* **8**, 054015 (2017).
- [32] Derivative of a quasiflux between circuit nodes 1 and 2 gives the respective voltage,  $\dot{\Phi}_{12} = U_{12}$  [45].
- [33] D. V. Anghel, K. Kulikov, Y. M. Galperin, and L. S. Kuzmin, Electromagnetic radiation detectors based on Josephson junctions: Effective hamiltonian, *Phys. Rev. B* **101**, 024511 (2020).
- [34] H.-P. Breuer and F. Petruccione, *The Theory of Open Quantum Systems* (Oxford University Press, New York, 2002).
- [35] J. Ping, X.-Q. Li, and S. Gurvitz, Quantum coherence and entanglement induced by the continuum between distant localized states, *Phys. Rev. A* **83**, 042112 (2011).
- [36] G. Zhu, D. G. Ferguson, V. E. Manucharyan, and J. Koch, Circuit qed with fluxonium qubits: Theory of the dispersive regime, *Phys. Rev. B* **87**, 024510 (2013).
- [37] M. Alexanian and S. K. Bose, Unitary transformation and the dynamics of a three-level atom interacting with two quantized field modes, *Phys. Rev. A* **52**, 2218 (1995).
- [38] Y. Wu, Effective raman theory for a three-level atom in the  $\Lambda$  configuration, *Phys. Rev. A* **54**, 1586 (1996).
- [39] J. M. Martinis, K. B. Cooper, R. McDermott, M. Steffen, M. Ansmann, K. D. Osborn, K. Cicak, S. Oh, D. P. Pappas,

- R. W. Simmonds, and C. C. Yu, Decoherence in Josephson Qubits from Dielectric Loss, *Phys. Rev. Lett.* **95**, 210503 (2005).
- [40] L. D. Landau and E. Lifshits, *Quantum Mechanics: Non-Relativistic Theory* (Butterworth-Heinemann, New York, 1991).
- [41] F. W. Strauch, Ph.D. thesis, School University of Maryland (2004).
- [42] J. M. Martinis, S. Nam, J. Aumentado, K. M. Lang, and C. Urbina, Decoherence of a superconducting qubit due to bias noise, *Phys. Rev. B* **67**, 094510 (2003).
- [43] A. Poudel, R. McDermott, and M. G. Vavilov, Quantum efficiency of a microwave photon detector based on a current-biased Josephson junction, *Phys. Rev. B* **86**, 174506 (2012).
- [44] M. Schöndorf, L. C. G. Govia, M. G. Vavilov, R. McDermott, and F. K. Wilhelm, Optimizing microwave photodetection: Input–output theory, *Quantum Sci. Technol.* **3**, 024009 (2018).
- [45] M. H. Devoret, *Quantum Fluctuations in Electrical Circuits*, in *Quantum Fluctuations* (Elsevier, New York, 1997), Chap. 10.